

The application of asymptotic analysis for modes I and III semi-infinite wedge solutions to a circumferentially notched shaft

P Duó*, A M Korsunsky, and D A Hills

Department of Engineering Science, University of Oxford, Oxford, UK

The manuscript was received on 8 June 2004 and was accepted after revision for publication on 12 October 2004.

DOI: 10.1243/030932405X12849

Abstract: Mode I and mode III solutions for sharp notch roots are derived and compared with representative full-field solutions. The example geometry studied is a circumferentially notched shaft, loaded in both tension and torsion. The calibration for the notch root intensity factors has been carried out using the finite element method. The combined effects of tension and torsion have been briefly considered as an example.

Keywords: asymptotes, antiplane shear, mode mixity, mode III, notch

1 INTRODUCTION

Asymptotic methods are a useful tool in stress analysis [1]. They enable the state of stress at (usually) a singular point to be encapsulated by a characteristic form. This is invaluable both analytically and as a means of evaluating the possibility of fatigue or monotonic fracture emanating from the point in question. The best-known family of solutions of this form are those relating to crack tips, where the applied load is decomposed into three standard forms, viz. symmetric or opening-mode (I), antisymmetric or shear mode (II), and antiplane mode (III). Each component of applied load contributes a characteristic eigensolution to the stress state, which exhibits a square-root singularity in the local radial coordinate and has a characteristic polar variation. The application of these solutions to the prediction of crack extension conditions under both monotonic and cyclic loading is well understood [2]. The eigensolutions may be derived in several different ways; the most popular one is to take the Westergaard solution for a crack in an infinite plane [3] and to take the limit when the radial coordinate from the crack tip becomes small compared with the crack length. An alternative, more fundamental,

technique is to solve for the semi-infinite crack itself, and this, in turn, may readily be derived from the solution for a semi-infinite 'wedge' or notch, first analysed by Williams [4]. The Williams solution shows that the stress state in the neighbourhood of the root is of power order form near the tip and has a characteristic spatial variation. Both modes I and II loading are treated. This has application to the study of sharp notch roots more generally, and the subject of 'notch mechanics' has evolved as a parallel to fracture mechanics [1]. The subject is less well known and is less well developed, but the intention is to provide a framework for the prediction of crack nucleation from notches, so that cross-correlation of the behaviour of notches in different components is possible, assuming that 'small-scale yielding' conditions exist. This simply means that the process zone at the notch root must be sufficiently small for all free surfaces other than the notch flanks to be ignored, i.e. that the semi-infinite solution correctly describes an elastic hinterland, and the philosophy is precisely the same as that introduced by Rice and Rosengren in fracture mechanics [5].

There does not appear to be a corresponding mode III solution for notch loading in the literature, which is surprising as the formulation is clearly simpler than that for modes I and II. The intention in the present paper is first to derive such a solution and to compare it with the characteristics of the modes I and II solution. This will then be applied, as an example, to a circumferentially notched bar loaded

*Corresponding author: Department of Engineering Science, University of Oxford, Parks Road, Oxford OX1 3PJ, UK. email: pierangelo.duo@eng.ox.ac.uk

in tension (mode I) and torsion (mode III). The limit of 'small-scale yielding' will be explored and the nature of the process zone when combined loading is applied will be found.

2 FORMULATION

2.1 Modes I and II

The complete solution was derived in Williams [4], with a complete description in reference [1]. Therefore, for brevity, only the eigenvalues λ_1 and λ_2 will be given here. If the included angle at the notch root is 2α , the state of stress in the neighbourhood of the root varies as $\rho^{\lambda-1}$, where ρ is a radial coordinate and λ is given by

$$\sin 2\lambda\alpha \pm \lambda \sin 2\alpha = 0 \quad (1)$$

The symmetric solution is associated with the positive sign and the antisymmetric solution with the negative sign. The corresponding eigenvalues are plotted in Fig. 1. The symmetric solution is singular if $\alpha > \pi/2$ rad, while the antisymmetric solution is singular only if $\alpha > 128.7^\circ$. Further, the symmetric solution is always more strongly singular than the antisymmetric one for any given notch, so that, unless special precautions are taken to suppress the symmetric mode, the symmetric component will dominate the solution for sufficiently small ρ .

2.2 Mode III solution

Antiplane shear problems are governed, not by the biharmonic equation, but by Laplace's equation, i.e.

$$\Delta F(\rho, \phi) = 0 \quad (2)$$

where the function F is related to the stress components by

$$\tau_{\rho\phi} = -\frac{\partial F}{\partial \rho} \quad (3)$$

$$\tau_{\zeta\phi} = \frac{1}{\rho} \frac{\partial F}{\partial \phi} \quad (4)$$

Here (ρ, ϕ) is a polar coordinate set centred at the notch tip. Assume that $F(\rho, \phi)$, by analogy with the modes I and II problem, may be written in the variables-separable form $F(\rho, \phi) = \rho^{\lambda_{III}} T(t)$, so that

$$\Delta F(\rho, \phi) = \rho^{\lambda_{III}-2} \left(\lambda_{III}^2 T + \frac{\partial^2 T}{\partial \phi^2} \right) \quad (5)$$

from which

$$F(\rho, \phi) = \rho^{\lambda_{III}} (c_1 \cos \lambda_{III} \phi + c_2 \sin \lambda_{III} \phi) \quad (6)$$

The only non-zero stresses are given by

$$\begin{aligned} \tau_{\rho\phi} &= -\frac{\partial F}{\partial \rho} \\ &= -\lambda_{III} \rho^{\lambda_{III}-1} (c_1 \cos \lambda_{III} \phi + c_2 \sin \lambda_{III} \phi) \end{aligned} \quad (7)$$

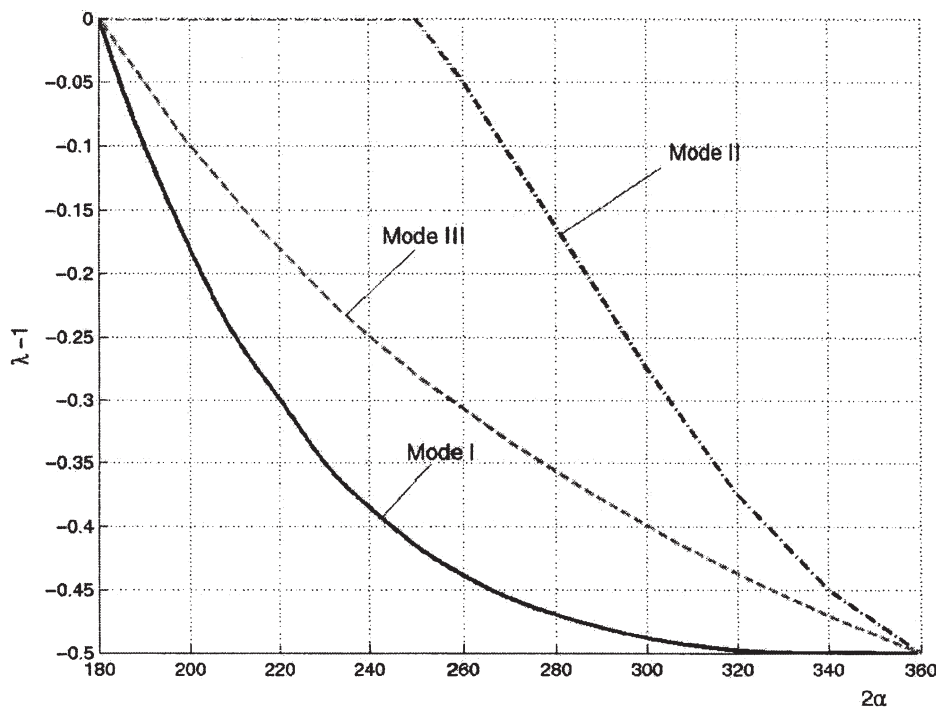


Fig. 1 Eigenvalues for mode I, mode II, and mode III solutions

$$\begin{aligned}\tau_{\zeta\phi} &= \frac{1}{\rho} \frac{\partial F}{\partial \phi} \\ &= \lambda_{III} \rho^{\lambda_{III}-1} (-c_1 \sin \lambda_{III} \phi + c_2 \cos \lambda_{III} \phi)\end{aligned}\quad (8)$$

Now set the traction component of stress ($\tau_{\zeta\phi}$) to zero on the faces $\phi = \pm\alpha$, to give the following characteristic equation

$$\sin 2\lambda\alpha = 0 \quad (9)$$

from which the relevant eigenvalue is given by

$$\lambda_{III} = \frac{\pi}{2\alpha} \quad (10)$$

Back-substitution, as before, yields the eigenfunction (i.e. the ratio c_1/c_2), and hence the spatial distribution of the non-zero shear stresses, which take on a particularly simple form. The solution is generally similar in behaviour to the symmetrical solution for the in-plane problem, and the eigenvalue is included in Fig. 1. It shows that all re-entrant wedges are singular, with, as expected, the strongest singularity (square root) when the wedge is folded to form a crack. For any given wedge angle the mode III singularity is *weaker* than the mode I solution, but is *stronger* than the mode II solution.

3 APPLICATION

As an example of the use of the technique, a study was made of the problem of a long circular shaft with a circumferential notch (Fig. 2) subject to remote

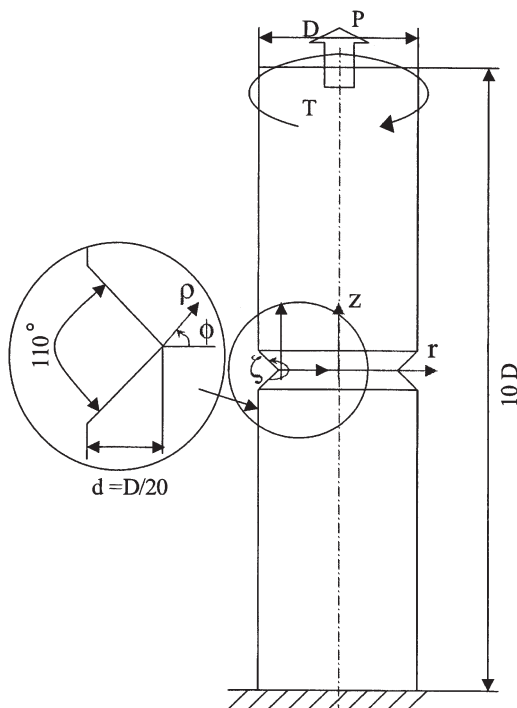


Fig. 2 The notched shaft problem used as an example. Note the local axis set centred on the notch root

tension and torsion. This has been treated by finite elements, using the commercial programme ANSYS. The figure depicts a shaft of diameter D , including a circumferential notch of depth $d = D/20$, and angle $\alpha = 125^\circ$. The length of the shaft is taken as $10D$ so that end effects are effectively suppressed. The problem was modelled with 5200 solid eight-noded axisymmetric elements, giving about 32 000 degrees of freedom. The mesh was very refined at the notch tip, but no additional precautions were taken to accelerate convergence of the solution, although the William's solution (see Fig. 1) shows that $\lambda_I - 1 = -0.42$ for the mode I solution and $\lambda_{III} - 1 = -0.28$ for the mode III solution just derived.

The generalized stress intensity factors for the problems based on the state of stress on the $\zeta = 0$ plane are defined so that the eigenfunctions become

$$\sigma_{ij}(\rho, \phi) = K_I^* \rho^{\lambda_I-1} f_{ij}(\phi) \quad (11)$$

$$\tau_{ij}(\rho, \phi) = K_{III}^* \rho^{\lambda_{III}-1} g_{ij}(\phi) \quad (12)$$

where, for the specific case $\alpha = 125^\circ$

$$\begin{Bmatrix} f_{\rho\rho} \\ f_{\phi\phi} \\ f_{r\phi} \end{Bmatrix} = \begin{Bmatrix} -\{0.65[\lambda_I(\lambda_I - 3)] \cos(\lambda_I - 1)\phi \\ + 0.424[\lambda_I(\lambda_I + 1)] \cos(\lambda_I + 1)\phi\} \\ \lambda_I(\lambda_I + 1)[0.65 \cos(\lambda_I - 1)\phi \\ + 0.424 \cos(\lambda_I + 1)\phi] \\ \lambda_I[0.65(\lambda_I - 1) \sin(\lambda_I - 1)\phi \\ + 0.424(\lambda_I + 1) \sin(\lambda_I + 1)\phi] \end{Bmatrix} \quad (13)$$

$$\begin{Bmatrix} g_{\rho\zeta} \\ g_{\zeta\phi} \end{Bmatrix} = \begin{Bmatrix} -1.3889\lambda_{III} \sin \lambda_{III}\phi \\ 1.3889\lambda_{III} \cos \lambda_{III}\phi \end{Bmatrix} \quad (14)$$

and the stress components are measured in a local axis set centred on the notch root (ρ, ϕ). The generalized stress intensity factors for the problem may therefore be found by extrapolating the relevant components of stress, i.e.

$$K_I^* = \rho^{-(\lambda_I-1)} \sigma_{\phi\phi}(\rho), \quad \lim \rho \rightarrow 0, \phi = 0 \quad (15)$$

$$K_{III}^* = \rho^{-(\lambda_{III}-1)} \tau_{\zeta\phi}(\rho), \quad \lim \rho \rightarrow 0, \phi = 0 \quad (16)$$

These extrapolations are displayed in Fig. 3(a) for a pure mode I loading and in Fig. 3(b) for a pure mode III loading. The values of the corresponding stress intensity factors, for the specific geometry of Fig. 2, were found to be $K_I^* = 1.02\sigma_0 d^{\lambda_I-1}$ and $K_{III}^* = 0.0078\tau_0 d^{\lambda_{III}-1}$, where

$$\sigma_0 = \frac{P}{\pi D^2} \quad (17)$$

$$\tau_0 = \frac{16T}{\pi D^3} \quad (18)$$

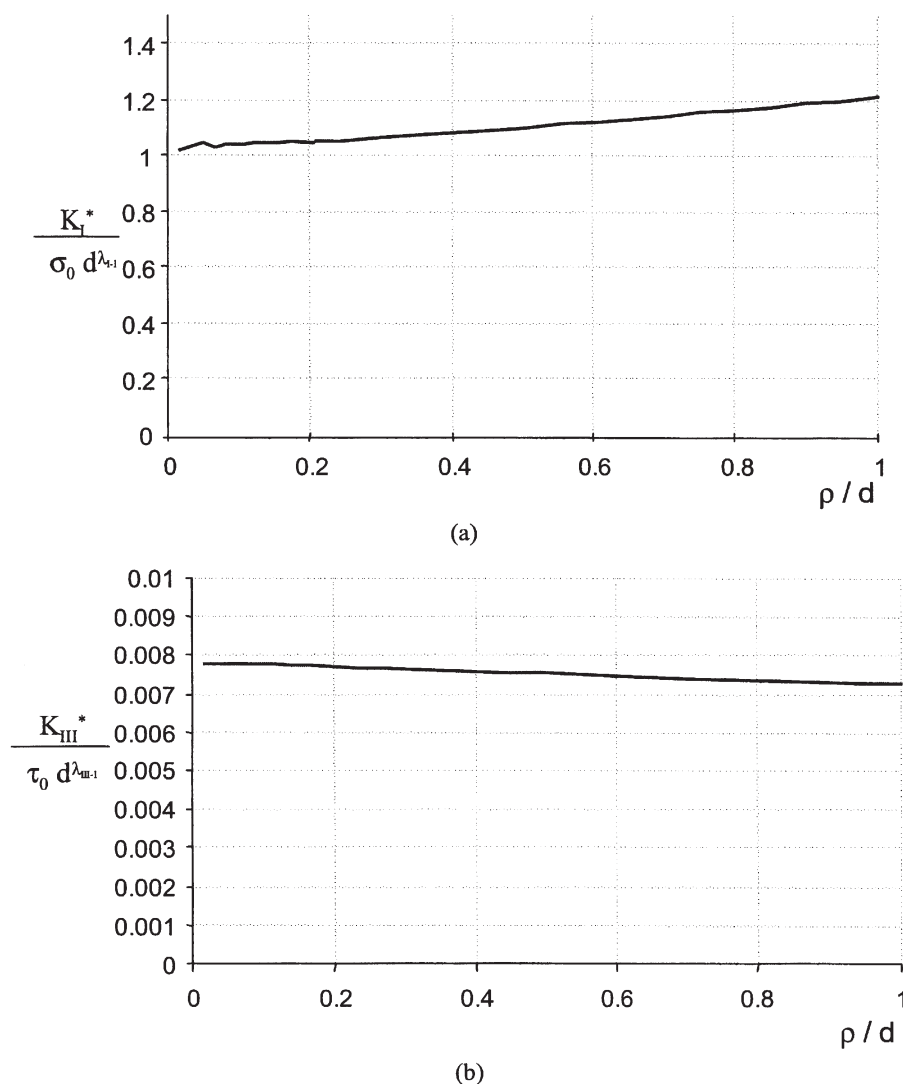


Fig. 3 Stress intensity factor calibration for the problem shown in Fig. 2: (a) pure mode I loading; (b) pure mode III loading

4 COMPARISON OF THE ASYMPTOTE AND THE FULL FIELD

Convergence of the results is displayed in Fig. 4(a) for a pure mode I loading. The full-field finite element (FE) results are plotted in dotted lines and for comparison the asymptote is shown in solid lines. A comparison between each of the system stress components would clearly be possible, but for brevity von Mises equivalent stress has been displayed, and the shape and size of the contours is very close for $\rho/d \leq 0.1$. Similarly, Fig. 4(b) gives contours of the von Mises parameter for the mode III component of loading alone. A comparison may be made between the asymptote shown in solid lines and the full stress field shown by dotted lines. Again, the similarity in the solutions is self-evident, with each containing a circular arc and a very clear matching of the asymptote and finite solution for $\rho/d \leq 0.3$.

5 PROCESS ZONES

The intended application of this analysis is to the quantification of the notch-root process zones, which are responsible for the nucleation of fatigue cracks, because of the irreversibilities that arise. It is therefore important to quantify the size of the process zone, in order to ensure that it lies well within the domain in which the elastic asymptote applies, i.e. small-scale yielding. Figure 4 provides information about the divergence between the asymptotic and full fields, and the other relevant information is therefore the position of the plastic front. In the spirit of fracture mechanics, where small-scale yielding is usually assumed, the plastic front will be established by using the elastic solution and noting where the yield criterion is exceeded. First the two modes of loading will be considered separately.

Two dimensionless load parameters m , n have been introduced to characterize both the magnitude

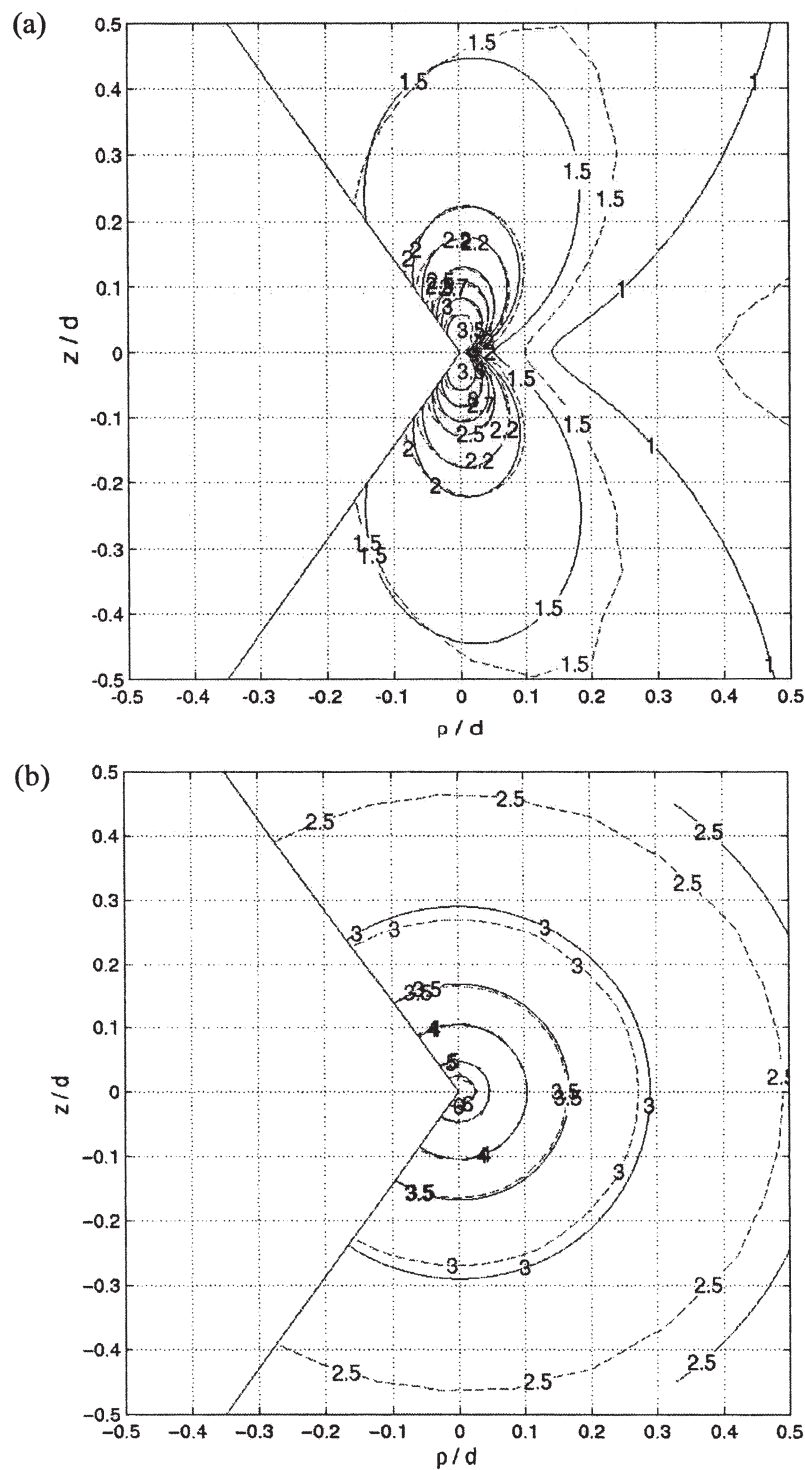


Fig. 4 Von Mises stress contours providing a comparison between full field and the asymptotic solutions: (a) pure mode I; (b) pure mode III

and contributions from the remotely applied loads. Let

$$\sigma_0 = mk \quad (19)$$

$$\tau_0 = nk \quad (20)$$

where k is the yield stress in pure shear. The stress intensity factors may now be written as

$$K_I^* = 1.02mkd^{1-\lambda_I} \quad (21)$$

$$K_{III}^* = 0.0078nk d^{1-\lambda_{III}} \quad (22)$$

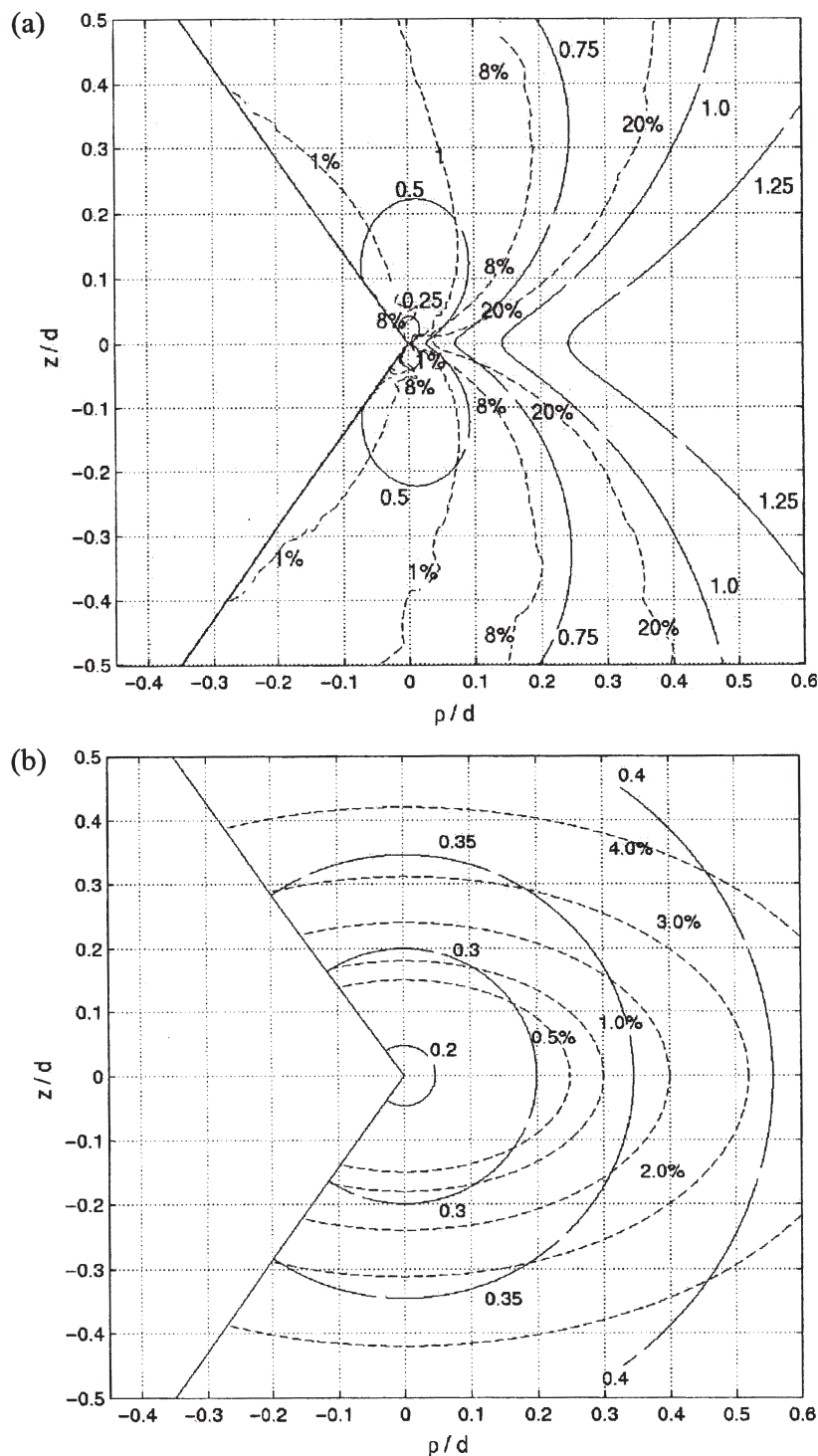


Fig. 5 Contours of plastic front position and mismatch between full field and asymptotic solutions: (a) in pure mode I, $m = 0.5-1.25$; (b) in pure mode III, $n = 0.2-0.4$

Figure 5 displays the position of the plastic front for various values of m , n . On the same figure plots are provided the discrepancy between the finite solution and the asymptote, deduced from Fig. 4, which are shown by broken lines. First, in relation to mode I loading, it will be noted that the 'error' (the difference between the two solutions) is relatively large along

$y = 0$, but small elsewhere. Figure 4 shows that, for any given radius ρ , the state of stress, as measured by the von Mises parameter, is much wider than at non-zero values of ϕ , so that the fractional difference is based on a small quantity. Thus, even though the shape and size of the process zones is small, the apparent error is large. On the other hand, in the

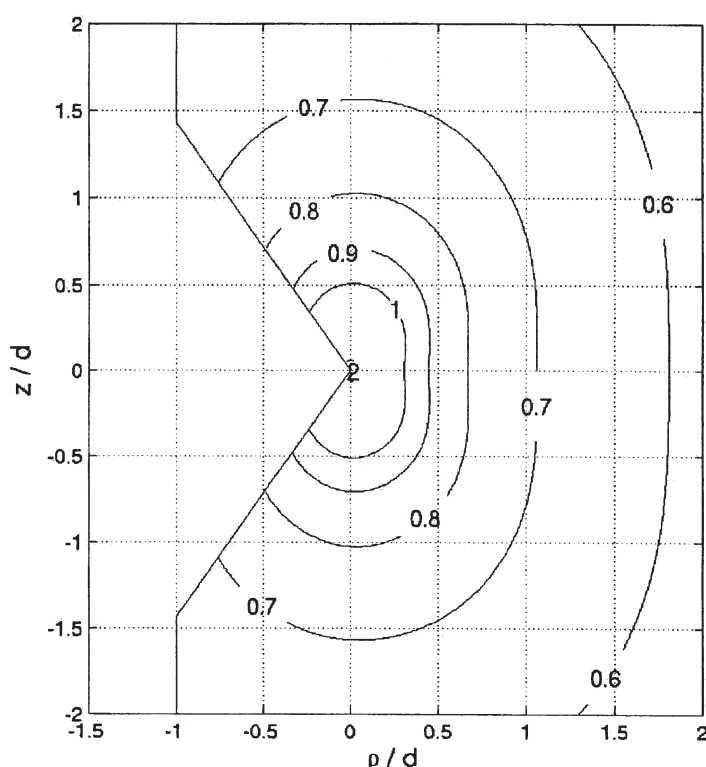


Fig. 6 Contours of plastic front position under mixed mode loading with $m = 0.7$, $n = 0.71$

case of mode III loading, the error contours are themselves circular, and hence, in order to ensure that the asymptote describes the solution correctly to within 4 per cent, for example, it is simply required that $n \leq 0.37$; this is not a practical limitation. Note that a discrepancy of 4 per cent is very much lower than that normally accepted in crack problems.

6 COMBINED MODES LOADING

When both modes of loading are combined the resultant state of stress may be found by superposition. This is defined by (K_{III}/K_I) , but it should be noted that this is not a dimensionless quantity (except in the special case of $\alpha \rightarrow \pi$, i.e. a crack) and it has dimensions of $[L^{\lambda_{III}-\lambda_I}]$. Thus, from equations (21) and (22)

$$\frac{K_{III}}{K_I} = \frac{0.0078}{1.02} \left(\frac{\tau_0}{\sigma_0} \right) d^{\lambda_{III}-\lambda_I} \quad (23)$$

$$\frac{\tau_0}{\sigma_0} = \frac{16T}{\pi D^3} \frac{\pi D^2}{P} = \frac{16T}{DP} \quad (24)$$

so that

$$\frac{K_{III}}{K_I} = 1.9576 \left(\frac{T}{P} \right) \frac{d^{\lambda_{III}-\lambda_I}}{D} \quad (25)$$

As an example, Fig. 6 shows the plastic zones present when $m = n = 0.71$, as established from the

asymptotes and, for comparison, as given by the numerical full-field solution.

7 CONCLUSION

A new general notch asymptote has been derived and applied to the problem of a circumferentially notched shaft. This has permitted the combined effect of modes I and III loading to be studied, together with precision. It is seen that the mode III asymptote is generally representative of the complete stress field over a rather larger region than mode I. It therefore forms an excellent potential means of correlating fatigue crack nucleation lives. A final word of caution must be added, pointed out by a diligent referee: unlike cracks, almost all notches are machined and hence must always be a finite root radius, even if small. For the asymptote to be valid this must be an order of magnitude smaller than the plastic radius.

REFERENCES

- 1 Aliabadi, M. H. and Rooke, D. P. *Numerical Fracture Mechanics*, 1991 (Kluwer Academic, Dordrecht, The Netherlands).
- 2 Ewalds, H. L. and Wanhill, R. J. H. *Fracture Mechanics*, 1985 (Edward Arnold, London).

- 3 Gdoutos, E. E.** *Fracture Mechanics Criteria and Applications*, 1990 (Kluwer Academic, Dordrecht, The Netherlands).
- 4 Williams, M. L.** Stress singularities resulting from various boundary conditions in angular corners of plates in extension. *J. Appl. Mechanics*, 1952, **19**, 526–528.
- 5 Rice, J. R. and Rosengren, G. F.** Plane strain deformation near a crack in a power law hardening material. *J. Mechanics and Physics of Solids*, 1968, **16**, 1–12.

APPENDIX

Notation

d	circumferential notch depth
D	shaft diameter

k	yield stress in pure shear
K_I^*	generalized stress intensity factor in mode I
K_{III}^*	generalized stress intensity factor in mode III
m, n	dimensionless load parameters
P	applied force
T	applied torque
α	notch angle
λ_I	eigenvalue in mode I loading
λ_{III}	eigenvalue in mode III loading
ρ, ϕ, ζ	polar coordinate set
σ_0, τ_0	applied stresses
$\tau_{\rho\phi}, \tau_{\zeta\phi}$	traction components of stress